

# Temperature-dependent Electronic Spectral Functions from Band-Structure Unfolding

Jingkai Quan<sup>1,2</sup>, Min-Ye Zhang<sup>1,3</sup>, Nikita Rybin<sup>1,4</sup>, Marios Zacharias<sup>1,5</sup>, Xinguo Ren<sup>3</sup>, Hong Jiang<sup>6</sup>, Matthias Scheffler<sup>1</sup>, and Christian Carbogno<sup>1,7</sup>

<sup>1</sup>The NOMAD Laboratory at the Fritz-Haber-Institut der Max-Planck-Gesellschaft, Faradayweg 4-6, 14195, Berlin, Germany

<sup>2</sup>Max-Planck Institute for the Structure and Dynamics of Matter, Luruper Chausse 149, 22761, Hamburg, Germany

<sup>3</sup>Institute of Physics, Chinese Academy of Sciences, 3rd South Str. 8, Beijing 100190, China

<sup>4</sup>*Current address:* Skolkovo Institute of Science and Technology, Bolshoi bulvar 30, build.1, 121205, Moscow, Russia

<sup>5</sup>*Current address:* Univ Rennes, INSA Rennes, CNRS, Institut FOTON - UMR 6082, F-35000 Rennes, France

<sup>6</sup>Beijing National Laboratory for Molecular Sciences, College of Chemistry and Molecular Engineering, Peking University, 100871 Beijing, China

<sup>7</sup>*Current address:* Theory Department, Fritz Haber Institute of the Max Planck Society, Faradayweg 4-6, 14195 Berlin, Germany

## Summary

The electronic band structure  $\varepsilon_n(\mathbf{k})$ , which describes the periodic dependence of the electronic quantum states  $n$  on the lattice momentum  $\mathbf{k}$  in reciprocal space, is one of the fundamental concepts in solid-state physics. It is key to our understanding of solid-state devices, since it allows rationalizing the electronic properties of periodic materials, e.g., to discern semiconductors with a direct band gap from those with an indirect one. In spite of that, the electronic band structure  $\varepsilon_n(\mathbf{k})$  is actually only well-defined for static nuclei, i.e., immobile nuclei fixed at their crystallographic positions. This constitutes a severe approximation that does not even hold in the limit of zero Kelvin due to the quantum-nuclear zero-point motion. To account for these thermodynamics effects, the band-structure concept can be generalized by introducing a temperature-dependent ( $T$ ) spectral-function  $\langle A(\mathbf{k}, E) \rangle_T$ , as shown in Fig. 1. In this case, the electronic quantum states at each reciprocal-vector  $\mathbf{k}$  are no longer sharp values  $\varepsilon_n(\mathbf{k})$ , but are characterized by a finite-width distribution. Several fundamental physical properties and mechanisms can only be understood and computed when the coupling between nuclear and electronic degrees of freedom is accounted for.

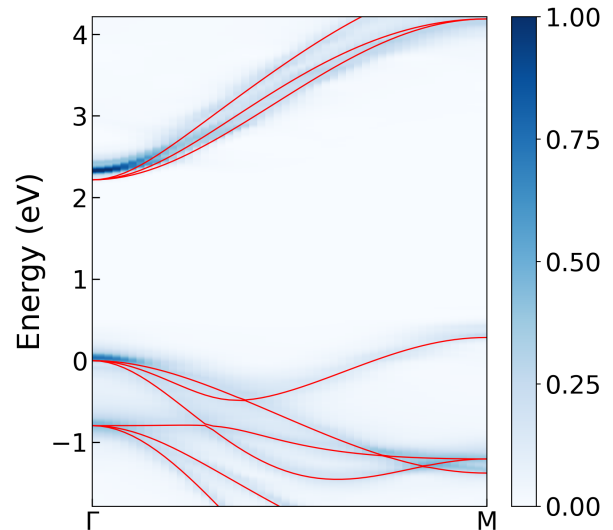


**Figure 1:** Electronic spectral function at 300K and the static band structure (red lines) of SrTiO<sub>3</sub>.

For instance, this includes the temperature-dependence of key electronic properties such as the band gap [1, 2, 3, 4], optical absorption spectra [5, 6], and electronic transport coefficients [7, 8, 9], also see Contrib. 7.2.

One possible route to compute spectral functions and the associated observables is many-body perturbation theory, a formally elegant and computationally efficient framework for treating electron-phonon coupling that is applicable within and beyond the Born-Oppenheimer approximation [10]. However, both the dynamics of the nuclei and that of the electrons are treated approximately in these methods by using the harmonic approximation for the nuclear degrees of freedom, also see Contribs. 6.1 and 7.1, and expressing the electronic response (including some second-order effects [10]) in terms of linear-order electron-phonon coupling elements. These approximations may well fail at elevated temperatures and/or for mobile atoms. For instance, it has been demonstrated that the complete concept of phonons can break down in systems exhibiting spontaneous defect formations, even if these defects are short-lived [11]. To avoid potential inaccuracies from the aforementioned approximations, the electronic spectral function can be equally obtained in a non-perturbative fashion within the Born-Oppenheimer approximation, hence capturing higher-order couplings between electronic and vibrational degrees of freedom. To this end, *ab initio* molecular dynamics (*aiMD*) can be run to accurately sample the full anharmonic potential-energy surface. The spectral-function is then obtained as the thermodynamic average  $\langle A(\mathbf{k}, E) \rangle_T$  of the instantaneous electronic-band structures  $\varepsilon_n(\mathbf{k})$  observed during this dynamics [12, 13, 14, 15].

From an electronic-structure point of view, one major hurdle in the implementation of the non-perturbative method arises from the fact that accurately sampling the dynamics in solids requires extended supercells, see Contrib. 6.1. However, the electronic band-structures' topology is fundamentally connected to the translational symmetries of a crystal, which results in band-structure folding in supercell electronic-structure theory calculations. In this case, electronic states associated to different  $\mathbf{k}$ -vectors in the first Brillouin zone are mapped onto the same  $\mathbf{K}$ -vector in the reduced Brillouin zone when extended supercells are used in real space, see Fig. 2. Accordingly, the utmost topological information is lost if the spectral function is computed as simple average over folded supercell band structures. Rather, it is necessary to first recover the representation in the first Brillouin zone, a process often referred to as *unfolding* [16, 17, 18, 19, 20] and visualized in Fig. 2. In this contribution, we shortly describe the implementation of the band-structure unfolding technique in the electronic-structure theory package *FHI-aims* and the updates made since its original development [12].

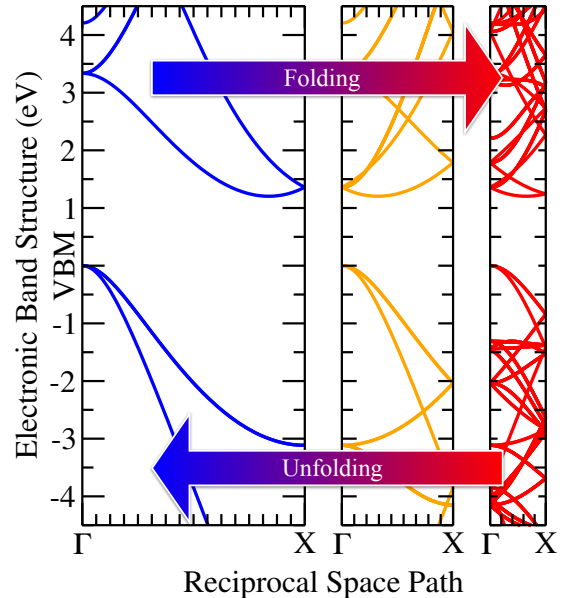


**Figure 2:** Folding viz. unfolding visualized for the HSE06 band structure of silicon along the high-symmetry  $\Gamma \rightarrow X$  path for the primitive unit cell (left), an eight-atom cubic conventional cell (middle), and a 64-atom cubic supercell (right).

## Current Status of the Implementation

The main difficulty in the implementation of band-unfolding techniques in *FHI-aims* stems from the usage of a non-orthogonal, atomic-centered basis. In this numeric atomic-orbitals (NAO) basis, atom displacements also affect the basis functions, so that changes in the basis set and in the overlap matrix need to be incorporated in the unfolding weight derivation [12]. We discuss the unfolding technique by establishing a relationship between the electronic structure obtained for a primitive cell (PC) and the

one obtained for a supercell (SC). Notationwise, properties associated to the PC or SC are denoted by using lower- and upper-case letters, respectively, and/or PC and SC subscripts when needed for clarity. Accordingly, the PC is characterized by the set of lattice vectors  $\underline{\mathbf{a}} = (\mathbf{a}_1, \mathbf{a}_2, \mathbf{a}_3)$  and the supercell (SC) by the lattice vectors  $\underline{\mathbf{A}} = \underline{\mathbf{a}} \cdot \underline{\mathbf{M}}$ . Here, the lattice vectors  $\mathbf{a}$  and  $\mathbf{A}$  are column vectors, as by FHI-aims convention, and the  $\underline{\mathbf{M}}$  is a non-singular matrix with integer entries, implying that the volume of the SC is  $m = |\det(\underline{\mathbf{M}})|$  times larger than that of the PC. Similarly, the lattice vectors  $\underline{\mathbf{b}}$  of the first Brillouin zone (BZ) associated with the PC and the ones of the reduced BZ associated with the SC are related via  $\underline{\mathbf{B}} = \underline{\mathbf{M}}^{-1} \underline{\mathbf{b}}$ . In turn, the volume of the reduced BZ is  $m$  times smaller than that of the first BZ, so that  $m$  different  $\mathbf{k}$ -vectors in the first BZ zone are mapped onto one and the same  $\mathbf{K}$ -vector in the reduced BZ. The unfolding technique reverses this mapping and re-establishes a representation in the first BZ.

To perform the mapping, the projection operator

$$\underline{\mathbf{P}}_{\mathbf{k}} = |\mathbf{k}\rangle \langle \mathbf{k}| \quad (1)$$

is used. Here,  $|\mathbf{k}\rangle$  are the eigenvectors with eigenvalue  $\exp(i\mathbf{k} \cdot \mathbf{a})$  that solve the eigenvalue problem<sup>1</sup>

$$\mathbf{t} |\mathbf{k}\rangle = \exp(i\mathbf{k} \cdot \mathbf{a}) |\mathbf{k}\rangle \quad (2)$$

for the translational operators  $\mathbf{t}$  associated to the lattice vectors  $\mathbf{a}$ . With that, it is possible to obtain the weights

$$W_{\mathbf{K}N}^{\mathbf{k}} = \langle \Psi_{\mathbf{K}N} | \underline{\mathbf{P}}_{\mathbf{k}} | \Psi_{\mathbf{K}N} \rangle = |\langle \mathbf{k} | \Psi_{\mathbf{K}N} \rangle|^2, \quad (3)$$

i.e., the contribution stemming from the subspace spanned by  $|\mathbf{k}\rangle$  associated with the translational symmetry of the PC to the SC wave function  $\Psi_{\mathbf{K}N}$ . For a “perfect” SC, i.e., one consisting of identical PC replicas, these weights are either 0 or 1, and one can hence reconstruct the exact band structure in the first BZ from a SC calculation. For a disturbed SC, the weights  $W_{\mathbf{K}N}^{\mathbf{k}}$  become fractional, since the SC system is not invariant under PC-translations  $\mathbf{t}$ . Accordingly, the desired remapping can be obtained by summing over all SC wave functions  $\Psi_{\mathbf{K}N}$  and computing the electronic spectral function

$$A(\mathbf{k}, E) = \sum_{\mathbf{K}N} W_{\mathbf{K}N}^{\mathbf{k}} \delta(E - E_{\mathbf{K}N}). \quad (4)$$

In practice, the unfolding implementation in FHI-aims start from the representation of the wave function  $\Psi_{\mathbf{K}N} = \sum_i C_{Ni}(\mathbf{K}) \chi_i(\mathbf{K})$  in the SC, where  $C_{Ni}(\mathbf{K})$  denotes a Kohn-Sham expansion coefficient and  $\chi_i(\mathbf{K})$  is a Bloch-like basis function build from numeric atomic orbitals. More details on these definition and notation can be found in Contrib. 1.1. In this SC Bloch-like basis, the algebraic representation of the PC translational operator is then constructed via  $t_{ij} = \langle \chi_i(\mathbf{K}) | \mathbf{t} | \chi_j(\mathbf{K}) \rangle$ . Let us emphasize that these functions are not orthogonal in real space, i.e., the overlap matrix  $S_{ij}(\mathbf{K}) = \langle \chi_i(\mathbf{K}) | \chi_j(\mathbf{K}) \rangle \neq \delta_{ij}$  is not diagonal. Accordingly, Eq. (2) becomes a generalized eigenvector problem in this representation, also see Contrib. 2.5. Its solution yields the eigenvalues  $\exp(i\mathbf{k} \cdot \mathbf{a})$ , i.e., those set of  $\mathbf{k}$ -points in the first BZ that this  $\mathbf{K}$ -point in the reduced BZ can be mapped to, and the set of eigenvectors  $\mathbf{k} = \sum_i F_i(\mathbf{k}) \chi_i(\mathbf{K})$  that are needed for constructing the projection operator  $\underline{\mathbf{P}}_{\mathbf{k}}$  defined in Eq. (1). With that one obtains the following formula for the weight

$$W_{\mathbf{K}N}^{\mathbf{k}} = |\mathbf{F}^\dagger(\mathbf{k}) \underline{\mathbf{S}}_{\mathbf{K}} \mathbf{C}_N(\mathbf{K})|^2 = |\mathbf{F}'^\dagger(\mathbf{k}) \mathbf{C}'_N(\mathbf{K})|^2. \quad (5)$$

In the last step, we have introduced the orthogonal representation  $\mathbf{C}'_N(\mathbf{K}) = \underline{\mathbf{S}}_{\mathbf{K}}^{1/2} \mathbf{C}_N(\mathbf{K})$  and  $\mathbf{F}'(\mathbf{k}) = \underline{\mathbf{S}}_{\mathbf{K}}^{1/2} \mathbf{F}(\mathbf{k})$  via a Löwdin transformation. Although the square root calculation  $\underline{\mathbf{S}}_{\mathbf{K}}^{1/2}$  constitutes a computational overhead, the latter orthogonal representation is advantageous, since this allows to find

<sup>1</sup>For the sake of clarity, the derivation here assumes non-degenerate eigenvalues. A discussion of the more general case including degeneracy can be found in Ref. [15].

analytical expressions of the eigenvector expansion coefficients  $\mathbf{F}'(\mathbf{k})$  at each  $\mathbf{K}$ -point in the reduced BZ [15]. With that the numerical solution of the eigenvalue problem in Eq. (2) is circumvented, leading to an overall speed-up of the procedure. Eventually, let us note that translations in three-dimensional systems form an Abelian group, so that the translations  $\mathbf{t}_\alpha$  associated to different lattice vectors  $\mathbf{a}_\alpha$  can be tackled consecutively.

## Usability and Tutorials

The overall workflow for computing temperature-dependent spectral functions  $\langle A(\mathbf{k}, E) \rangle_T$  is sketched in Fig. 3. First, one or multiple *aiMD* runs are performed in a SC at temperature  $T$  to sample the thermodynamic phase-space. From these trajectories,  $L$  single, uncorrelated “samples”, i.e., atomic configurations  $\mathbf{R}_I^{\text{SC}}(t_l)$  at sufficiently distant times  $t_l$ , are extracted and their electronic band-structure  $\varepsilon_N(\mathbf{K}, t_l)$  is computed at a sufficiently dense  $\mathbf{K}$ -grid. In this step, the unfolding routines are used to map back the band-structure  $\varepsilon_N(\mathbf{K}, t_l)$  onto the first BZ, i.e., the weights  $W_{\mathbf{K}\mathbf{N}}^{\mathbf{k}}(t_l)$  are computed and stored on file together with  $\varepsilon_N(\mathbf{K}, t_l)$ . In the last steps, the outputs are post-processed by computing the spectral functions  $A(\mathbf{k}, E, t_l)$  of the individual samples, see Eq. (4), and by eventually computing the thermodynamic average

$$\langle A(\mathbf{k}, E) \rangle_T = \frac{1}{L} \sum_{l=1}^L A(\mathbf{k}, E, t_l). \quad (6)$$

A more detailed description including scripts to pre- and post-process the calculations and to analyze the data are given in the tutorial at <https://fhi-aims-club.gitlab.io/tutorials/band-unfolding>. In this context, let us note that the method is not strictly restricted to *aiMD*, but any kind of sampling method can be used to explore the relevant phase-space. For instance, path-integral MD, see Contrib. 6.3 can be used instead, if it is necessary and desirable to account for quantum-nuclear effects. Along this lines, also more approximative methods, e.g., harmonic sampling as implemented in *FHI-vibes* [21] and described in Contrib. 6.1 or MD on machine-learned interatomic potentials as described in Contrib. 8.4, can in principle be used. In such cases, however, correct spectral functions can only be obtained if the employed approximations hold, as discussed in the respective contributions.

In more detail, the unfolding procedure in *FHI-aims* is part of the native band-structure post-processing tool. Accordingly it is invoked by using the keyword `output band` to define the reciprocal-space path for the SC, i.e., the  $\mathbf{K}$ -points that shall be targeted and by setting the keyword `bs_unfolding` in the `control.in` file. Additionally, two more input files are required: `transformation_matrix.dat`, where one defines the transformation matrix  $\underline{\mathbf{M}}$  between PC lattice vector  $\underline{\mathbf{a}}$  and SC lattice vector  $\underline{\mathbf{A}}$ , and `unfolding_map.dat`, describing the mapping between atoms in the PC and the SC that is later used for constructing the translational operator  $\mathbf{t}$ . The latter is an index map  $I \rightarrow j$  that relates the atomic coordinates in an unperturbed supercell  $\mathbf{R}_I^{\text{SC}} = \mathbf{R}_j^{\text{PC}} + \sum_\alpha n_\alpha \mathbf{a}_\alpha$   $n_\alpha \in \mathbb{Z}$  to the ones of the atoms  $\mathbf{R}_j^{\text{PC}}$  in a primitive cell. Upon completion, the unfolding weights for each SC  $\mathbf{K}$ -point are written into separate files named `unfold_k_###.out` using the same `NXY` format used in the standard band

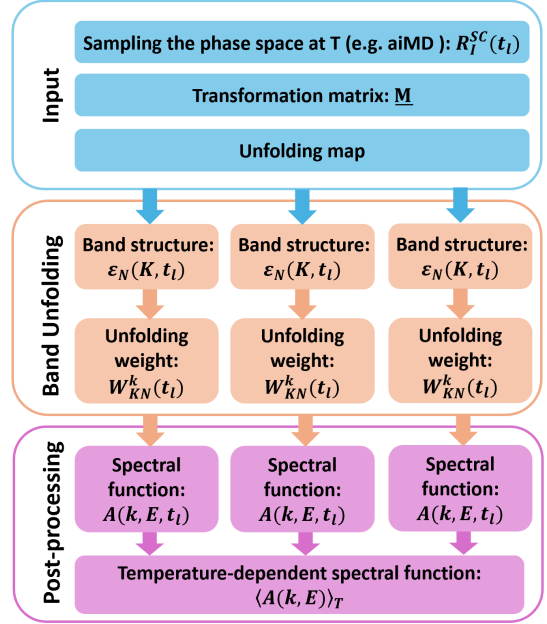


**Figure 3:** Schematics of a typical workflow used to obtain temperature-dependent spectral functions  $\langle A(\mathbf{k}, E) \rangle_T$ .

structure output.

Currently, the band-unfolding implementation in FHI-aims supports all Bravais lattice, all exchange-correlation functionals, and all type of transformation matrices  $\underline{\mathbf{M}}$ , including non-diagonal ones typically needed to map primitive fcc and bcc structures to conventional cubic supercells. Both support for LAPACK and ScaLAPACK is implemented, allowing for a trivially parallel parallelization over  $\mathbf{K}$ -points in the case of small systems requiring many  $\mathbf{K}$ -points (LAPACK) and for a block cyclic distribution and distributed linear algebra in the case of large systems with few  $\mathbf{K}$ -points (ScaLAPACK). With that, the band unfolding implementation in FHI-aims can routinely handle large supercells with small computational overhead. For instance, the unfolding only requires approx. 20% of the total runtime when computing a 4,096-atom Silicon with one k-point,  $> 100,000$  basis functions and  $> 40,000$  states at the semi-local level of exchange-correlation.

Eventually, let us note that also *electron-electron* coupling, i.e., electronic many-body effects, can play an important role for spectral functions [22, 23]. To this end, the current implementation also supports the unfolding of  $G_0W_0$  calculations. In this case, the complex-valued self-energy is treated as a correction to the orbital energy, while the wave function is assumed to remain as in the Kohn-Sham scheme. The unfolded spectral function can then be computed in close analogy to Eq. (4). The required weights are obtained at the Kohn-Sham level, while the delta-function  $\delta(E - E_{\mathbf{K}N})$  is replaced by the spectral function obtained at the  $G_0W_0$  level. By this means, electron correlation is explicitly accounted for. As an example, Fig. 4 shows the unfolded  $G_0W_0$  band structure for a perfect  $2 \times 2 \times 2$  silicon super cell.

### Future Plans and Challenges

As described in this contribution, the band-structure unfolding procedures implemented in FHI-aims enable a routine assessment of temperature-dependent spectral functions both at the density-functional theory and at the  $G_0W_0$  level. From a workflow perspective, the presented methodology is independent on the actual methodologies used (i) for accurately sampling the thermodynamic phase-space and (ii) for obtaining the electronic band-structures  $\varepsilon_N(\mathbf{K})$  in the SC, as detailed above. With that, the availability of (sufficiently accurate) machine-learned interatomic potentials [24] and of (sufficiently accurate) machine-learned electronic-structure theory [25, 26, 27], see Contribs. 8.4 and 8.5, can give access to much larger system sizes. Performance-wise, already the current implementation can handle such cases. However, access to such larger system sizes also enables the study of new physical questions, e.g., the influence of point defects, of grain boundaries, and of solid-solid interfaces. While the overall theory holds also in such cases, the construction of the translational  $t$  operator will require case-specific adaptations to reflect the different types of breaking in translational symmetry.

Furthermore, the above-mentioned machine-learning methods might even help to solve a more fundamental open question with respect to non-adiabatic effects [28], which can play a fundamental role for spectral functions, as evidence from many-body perturbation theory shows [29]. So far, however, such kind of effects could not be studied with the herein presented non-perturbative approach, since

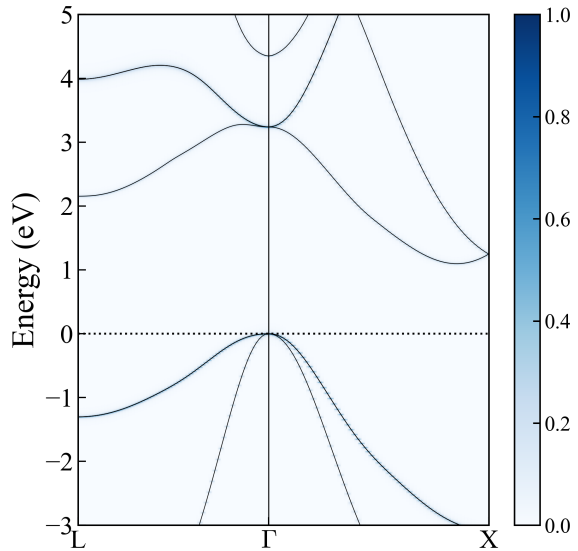


**Figure 4:**  $G_0W_0$  spectral function (blue) for a perfect  $2 \times 2 \times 2$  silicon super cell unfolded onto the first Brillouin zone. The  $G_0W_0$  band structure obtained in a PC is shown as comparison in black.

it would require prohibitively expensive time-dependent electronic-structure theory calculations. With the advent of such machine-learning methods, this hurdle may fall and hence allow to study the connection between anharmonic and non-adiabatic effects.

## Acknowledgements

This work was supported by the NOMAD Center of Excellence (European Union's Horizon 2020 research and innovation program, Grant Agreement No. 951786), TEC1p (the European Research Council (ERC) Horizon 2020 research and innovation programme, grant agreement No. 740233), and BigMax (the Max Planck Society's Research Network on Big-Data-Driven Mater.-Science).

## References

- [1] F. Giustino, S. G. Louie, and M. L. Cohen, *Phys. Rev. Lett.* **105**, 265501 (2010).
- [2] E. Cannuccia and A. Marini, *The Europ. Phys. Journal B* **85**, 320 (2012).
- [3] S. Ponce, G. Antonius, P. Boulanger, E. Cannuccia, A. Marini, M. Cote, and X. Gonze, *Comp. Mater. Science* **83**, 341 (2014).
- [4] M. Zacharias and F. Giustino, *Phys. Rev. Res.* **2**, 013357 (2020).
- [5] J. Noffsinger, E. Kioupakis, C. G. Van de Walle, S. G. Louie, and M. L. Cohen, *Phys. Rev. Lett.* **108**, 167402 (2012).
- [6] M. Zacharias, C. E. Patrick, and F. Giustino, *Phys. Rev. Lett.* **115**, 177401 (2015).
- [7] J. I. Mustafa, M. Bernardi, J. B. Neaton, and S. G. Louie, *Phys. Rev. B* **94**, 155105 (2016).
- [8] J.-J. Zhou, O. Hellman, and M. Bernardi, *Phys. Rev. Lett.* **121**, 226603 (2018).
- [9] S. Ponce, W. Li, S. Reichardt, and F. Giustino, *Rep. Prog. Phys.* **83**, 036501 (2020).
- [10] F. Giustino, *Rev. Mod. Phys.* **89**, 015003 (2017).
- [11] F. Knoop, T. A. R. Purcell, M. Scheffler, and C. Carbogno, *Phys. Rev. Lett.* **130**, 236301 (2023).
- [12] M. Zacharias, M. Scheffler, and C. Carbogno, *Phys. Rev. B* **102**, 045126 (2020).
- [13] J. P. Nery and F. Mauri, *Phys. Rev. B* **105**, 245120 (2022).
- [14] N. Rybin, PhD thesis, Humboldt-Universität zu Berlin, 2023.
- [15] J. Quan et al, *in preparation*, 2024.
- [16] T. B. Boykin and G. Klimeck, *Phys. Rev. B* **71**, 115215 (2005).
- [17] W. Ku, T. Berlijn, and C.-C. Lee, *Phys. Rev. Lett.* **104**, 216401 (2010).
- [18] V. Popescu and A. Zunger, *Phys. Rev. B* **85**, 085201 (2012).
- [19] P. B. Allen, T. Berlijn, D. A. Casavant, and J. M. Soler, *Phys. Rev. B* **87**, 085322 (2013).
- [20] X. Zhang, J. Kang, and S.-H. Wei, *Chin. Phys. Lett.* **41**, 026301 (2024).
- [21] F. Knoop, T. A R Purcell, M. Scheffler, and C. Carbogno, *J. Open Source Softw.* **5**, 2671 (2020).

- [22] G. Antonius, S. Poncé, P. Boulanger, M. Côté, and X. Gonze, *Phys. Rev. Lett.* **112**, 215501 (2014).
- [23] F. Karsai, M. Engel, E. Flage-Larsen, and G. Kresse, *New Journal of Phys.* **20**, 123008 (2018).
- [24] J. Behler and G. Csányi, *Europ. Phys. Journal B* **94**, 142 (2021).
- [25] H. Li, Z. Wang, N. Zou, M. Ye, R. Xu, X. Gong, W. Duan, and Y. Xu, *Nature Comp. Science* **2**, 367 (2022).
- [26] L. Zhang, B. Onat, G. Dusson, A. McSloy, G. Anand, R. J. Maurer, C. Ortner, and J. R. Kermode, *npj Comp. Mater.* **8**, 158 (2022).
- [27] A. M. Lewis, A. Grisafi, M. Ceriotti, and M. Rossi, *J. Chem. Theo. Comp.* **17**, 7203 (2021).
- [28] M. Lazzeri and F. Mauri, *Phys. Rev. Lett.* **97**, 266407 (2006).
- [29] A. Miglio *et al.*, *npj Comp. Mater.* **6**, 167 (2020).